Chloride-initiated corrosion in alkali activated reinforced concrete

MANGAT, Pal <http://orcid.org/0000-0003-1736-8891>, OJEDOKUN, Olalekan <http://orcid.org/0000-0002-9573-4976> and LAMBERT, Paul <http://orcid.org/0000-0002-2815-1674>

Published version

MANGAT, Pal, OJEDOKUN, Olalekan and LAMBERT, Paul (2021). Chloride-initiated corrosion in alkali activated reinforced concrete. Cement and Concrete Composites, 115, p. 103823.

Chloride-initiated corrosion in alkali activated reinforced concrete

P.S. Mangat, Olalekan O. Ojedokun and Paul Lambert

Centre for Infrastructure Management, Materials and Engineering Research Institute, Sheffield Hallam University, Sheffield S1 1WB, UK

Abstract

The use of ordinary Portland cement (PC) as the principal binder in concrete brings with it significant environmental challenges through the consumption of fossil fuels and emission of carbon dioxide (CO_2) during cement production. Concrete specimens made with an alkali activated cementitious material (AACM) produced from an alternative binder and conventional Portland cement concrete were exposed to corrosion inducing environments for 1750 days to monitor their relative durability. AACM concrete shows higher corrosion potential E_{corr} and corrosion current densities I_{corr} than PC concrete due to a reducing environment around the steel surface in AACM concrete, caused by high sulfide concentration in the pore solution. Corrosion resistance of the AACM concretes increases with increasing molarity of the alkali activator, at a constant liquid to binder ratio. The threshold Cl^-/OH^- value for pitting corrosion initiation in the AACM concrete is between 2.1 and 2.8 compared with 1.08 for the control PC concrete. The AACM concrete evaluated in this study showed greater resistance to chloride induced corrosion than the PC concrete.

Keywords: Alkali activated concrete, AACM concrete, corrosion potential E_{corr}, corrosion current density I_{corr}, chloride induced corrosion, free chloride/hydroxyl ion ratio, water capillary absorption.

Notations:

AACM	Alkali activated cementitious materials
PC	Portland cement
i_{corr}	Corrosion current density (μA/cm^2)
E_{corr}	Corrosion potential (mV)
A	Surface area of the exposed reinforcing steel (mm^2)
I	Galvanic current
Cl^-/OH^-	Chloride/hydroxyl ion concentration
ZRA	Zero-Resistance Ammeter

1.0 Introduction

The structural integrity of reinforced concrete may be undermined by the onset of corrosion of steel reinforcement, leading to a high cost of repair or replacement [1]. Chloride ingress and carbonation in concrete structures are the main causes of corrosion of steel reinforcement and fibres [2, 3]. There is the likelihood of a reduced impact of chloride induced corrosion in AACM concrete relative to PC concrete structures due to the lower rate of chloride ingress in the former [4] suggesting a longer time for onset of corrosion in reinforced AACM concrete.

Resistance against corrosion initiators such as chlorides in PC concrete is provided by a thermodynamically stable passive film formed at the steel-concrete interface when the pore solution pH is above 12.5 during cement hydration [5, 6]. The passive film has been shown to consist of an inner anhydrous oxide layer (Fe_2O_3 or Fe_3O_4) approximately 2.5nm thick and a 1nm outer hydrous layer [7]. The stability of the passive film is governed by the availability of oxygen at the steel-concrete interface, the level of alkalinity and chemistry of the concrete pore solution and the redox potential of the embedded steel [5, 8]. The breakdown of the passive film or de-passivation in AACM and PC concrete are expected to be different, largely due to differences in their pore solution chemistry. Studies [9] show that passivation of steel reinforcement in PC concrete during cement hydration is supported by Portlandite, $Ca(OH)_2$, which is not identified in AACM concrete [10, 11]. The pore matrix of AACM concrete contains high levels of alkalinity and a relatively poor oxidation environment which are considered to sustain passivity of embedded steel reinforcement [8]. There is limited information in the literature to validate this theory.

The redox potential at the steel-concrete interface is influenced by the presence of sulfide in the pore solution of the concrete [12]. Sulfide deposits on the steel surface have been observed to delay the oxidation reaction to a certain extent which reduces the rate of corrosion reaction

of the embedded steel [13]. Furthermore, oxidized sulfide was suggested to produce elemental sulfur which accumulates at the pores of the depleted passive film resulting in its repair [12], particularly at sufficiently high sulfide concentration [13]. Alternatively, Tromans [14] suggested a reduction in the passive film due to the attraction of sulfide by magnetite resulting in the disintegration of the passive film [15], thereby, promoting higher corrosion rates. Blast furnace slag has high sulfide content which produces redox potentials of negative values compared to PC concrete [12]. Therefore, the corrosion behaviour of AACM concrete may be expected to be significantly different from PC concrete. An investigation of the chloride induced corrosion behaviour of AACM and control PC concrete is reported in this paper to provide insight into the mechanism of this process, which is currently limited.

The distinctive pore properties of AACM concrete demonstrate lower porosity and chloride binding capacity compared with PC concrete [16]. The pore properties of AACM concrete were observed to show higher proportions of capillary pores (0.01 – 100μm) and lower proportions of gel pores (0.005 – 0.01μm) than PC concrete. Such pore size and distribution properties are likely to influence the availability or deprivation of oxygen and chloride ions at the steel-concrete interface. The onset of chloride induced corrosion of steel embedded in concrete is linked to what is commonly referred to as the chloride threshold, which is the minimum chloride concentration at the steel surface that triggers pitting corrosion. It is acknowledged that the critical chloride threshold does not exist as a single level, but this value varies greatly as it is influenced by variations in the mix design, age of concrete, type of steel reinforcement and construction practice [17, 18]. The inherent heterogeneous nature of the multi-phase matrix structure is considered to be a major reason for variation in chloride threshold values [19]. The curing environment also accounts for variation in the critical chloride threshold and corrosion behaviour of steel reinforced AACM concrete [12].

Most research has used accelerated electrochemical test methods to monitor corrosion behaviour of steel bars in simulated pore solutions of AACM concrete [5, 20, 21] while other factors such as porosity and chloride binding capacity of AACM concrete are neglected. The role of the concrete matrix in controlling the physical and chemical processes (e.g. diffusion and chloride binding) which produce the pore solution chemistry are not represented in these accelerated electrochemical tests. Performance validation of concrete-based materials should adopt test methods designed to give a true representation of material behaviour that cannot reliably be achieved using accelerated electrochemical test methods of steel in simulated pore solutions. The accelerated corrosion test method adopted in the authors' research avoids this limitation by exposing steel bars embedded in AACM and PC concrete matrices to accelerated corrosion inducing environments which include concentrated chloride solution, high temperature, moisture, low humidity exposure cycles to allow oxygen diffusion to the steel and accelerate chloride diffusion by capillary action.

In this study, three grades of AACM concrete representing low, medium and high strengths [16] are exposed to an accelerated corrosive environment involving, in sequence, immersion in 5% chloride solution at 20^0C; dry curing at 20^0C and 65% R.H.; exposure in an environmental chamber at 50^0C and 75% R.H. and 1 day wet/6 days dry curing cycles. The environment of exposure was selected to provide sufficient levels of chloride, oxygen and temperature to initiate corrosion within the timescale of the research. The investigation of the corrosion behaviour of steel reinforcement in AACM concrete under the relatively accelerated chloride induced corrosion environment will provide an understanding of its practical application potential in salt laden environments such as structures exposed to splash and tidal zones and de-icing salts.

2.0 Experimental programme

2.1 Materials and mixes

AACM concrete mixes (AACM 1, 2 and 3) made with the alkali activated cementitious material binder (AACM) and conventional PC concrete were produced as shown in Table 1. Ground granulated blast furnace slag (GGBS) and CEM 1 cement of grade 42.5R [22], supplied locally in Sheffield, UK were used as binders in the AACM and PC concrete mixes respectively. The chemical composition of the GGBS and CEM 1 cement is given in Table 2. The activator used in the AACM concrete is a sodium silicate solution of 6.5mol/L molarity and 2% modulus, together with NaOH of molarity 4.8mol/L. AACM 1, 2 and 3 mixes were produced by diluting the activator with water at 0%, 3.88% and 7.76% respectively as shown in Table 1, to produce low, medium and high strength grades [16, 23]. A liquid-binder ratio of 0.47, 10mm uncrushed gravel, 6mm limestone and a medium grade sand with 80% particle size passing 1mm sieve were used in both the AACM and PC concrete mixes. The properties and oxide compositions of these aggregates conform to BS 882:1992 [24]. Retarder R42 made from a blend of high grade polyhydroxy-carboxylic acid derivatives and a shrinkage reducing admixture (SRA) based on an alkyl-ether were added to the AACM mixes to improve their workability and setting time. Each chemical admixture contained less than 0.1% chloride ion and 3.5% sodium oxide.

Table 1: Composition of AACM 1, 2, 3 and control PC concrete mixes

Mix	Binder Content (%)	Fine Agg. (%)	Coarse Agg. (%)		Liquid/ Binder Ratio	Activator Dilution (%)	Activator Molarity mol/L	R42	SRA
			10mm Gravel	6mm Limestone				(% by weight of binder)	
AACM 1	25	18	29.3	15.7	0.47	0	6.50	0.2	0.5
AACM 2	25	18	29.3	15.7	0.47	3.88	6.26	0.2	0.5
AACM 3	25	18	29.3	15.7	0.47	7.76	6.0	0.2	0.5
Control PC	20	26	28.9	15.5	0.47(w/c)	-	-	-	-

*R42 is the retarder; SRA is the shrinkage reducing admixture

Table 2: Chemical composition of CEM 1 cement and GGBS binders

Chemical component	SiO_2	Al_2O_3	Fe_2O_3	CaO	MgO	K_2O	Na_2O	TiO_2	P_2O_5	MnO	SO_3
CEM 1 (mass %)	11.1	8.35	3.16	64.2	2.09	1.19	0.227	1.88	2.01	2.14	3.64
GGBS (mass %)	28.6	12.4	5.7	42.3	6.1	0.8	0.4	1.78	<0.1	0.3	0.08

2.2 Corrosion test specimen Preparation

Plain mild steel reinforcement bars of 8mm diameter conforming to BS 4449:2005+A3:2006 [25] were embedded in the AACM and PC concrete mixes. Their percentage chemical composition is 98.5% Fe, 0.22% C, 0.23% Si, 0.52% Mn, 0.01% P, 0.01% S, 0.30% Cr, 0.14% Ni, 0.04% Cu and 0.03% Mo. The steel bars were cut into 400mm lengths and then grit blasted to remove all mill scale, rust and contamination (Fig. 1). A 4mm thread was tapped at one end of each rebar to accommodate an electrical connection. Both ends of each steel bar were masked with an epoxy resin coating applied over cement paste cast over a length of 100mm from both ends, leaving an exposed surface area of 50cm^2. Care was taken to prevent the epoxy coating from coming in direct contact with the steel bar to prevent isolation of electrical connection and formation of a crevice.

a

b

Fig. 1: Reinforcing bars (a) before grit blasting (b) after grit blasting

Fig. 2: Reinforcing bars positioned in polystyrene moulds prior to casting

Triplicate steel bars were placed inside a polystyrene mould at a depth of 30mm (cover) from the bottom cast face as shown in Fig. 2. The opening around the steel bars in the polystyrene mould was completely sealed off to prevent leakage of concrete during casting. The polystyrene moulds were lightly oiled to prevent concrete from sticking followed by cleaning the steel with acetone to degrease and remove any dirt from the surface. Each polystyrene mould with the positioned triplicate steel bars was filled with concrete in three layers.

Fresh AACM and PC concretes were mixed in a 150 kg capacity Cretangle mixer in accordance with BS EN 206:2013+A1:2016 [22] and placed into the polystyrene moulds in three layers. Each layer was compacted on a vibrating table for up to 30 seconds to attain homogeneity and minimize the presence of voids. The cast specimens were placed on a flat table surface and covered with polyethylene sheets to prevent moisture loss. A total of eight 250 x 250 x 75 mm steel reinforced slabs were produced for the AACM and PC concretes, two specimens for each of AACM 1, 2, 3 and PC concrete. The specimens were cured in the laboratory at 20 ± 2°C and 65% R.H. for 24 hrs after casting and then demoulded. The hardened concrete was then cured in water (20 ± 2°C) for 27 days after demoulding. The specimens were taken out of water and surface dried after 28 days from casting. Two coats of bituminous paint were applied to five faces of each specimen, except the bottom cast face of 250mm x 250mm dimensions. The bituminous paint was allowed to dry for 24 hrs. The specimens were then exposed to the following accelerated corrosion inducing environment cycles as shown in Table 3.

Table 3: Exposure regime for AACM and PC concrete to induce corrosion

Exposure (days)	0 - 90	90 - 190	190 - 260	260 - 340	340 - 440	440 - 510	510 - 690	690 - 860	860- 1311	1311- 1440	1140- 1568	1568- 1750

Curing regime	Chloride diffusion	Dry curing	Chloride diffusion	Climate chamber	Chloride diffusion	Dry curing	Chloride diffusion	1 day wet/ 6 days dry cycle	Dry curing	Wet curing	Dry curing	Wet curing
Condition	(20+2^{0}C) 5% NaCl	(20+2^{0}C, 65R.H.)	(20+2^{0}C) 5% NaCl	(50^{o}C, 75% RH)	(20+2^{0}C) 5% NaCl	(20+2^{0}C, 65R.H.)	(20+2^{0}C) 5% NaCl	(20+2^{0}C) 65%RH	(20+2^{0}C, 65R.H.)	(40^{0}C)	(20+2^{0}C, 65R.H)	(40^{0}C)

2.3 Test procedures

2.3.1 Electrochemical monitoring

The corrosion potential E_{corr} and current density I_{corr} values were measured up to 1750 days under cycles of exposure given in Table 3. Half-cell potential monitoring of the AACM and PC corrosion specimens was performed using a reference electrode and digital voltmeter (DVM) in accordance with TR 60 [26] and ASTM C876 – 15 [27]. A silver-silver chloride (SSC) reference electrode was connected to a digital voltmeter for taking the potential readings in order to avoid contamination when immersed in NaCl solution, unlike a copper-copper sulphate electrode that is prone to such contamination [27].

Galvanic current density of the AACM and PC concrete was determined using a Zero-Resistance Ammeter (ZRA) from ACM instruments with a current range of 500mA and operational temperature range of -5^{0}C to 72^{0}C. A range of 100 µA was used to measure the galvanic current between two electrodes connected to the embedded triplicate steel bars and a stainless steel electrode with an area of 625 cm^2 placed on top of the corrosion specimens (Fig. 3). The readings of the galvanic current between the two electrodes became stable after 3 minutes. The corrosion current density was calculated from the readings as follows:

$$i_{corr} = {}^{I}/_{A} \qquad 1$$

where i_{corr} is the corrosion current density (µA/cm^2), A is the surface area of the uncoated section of embedded steel (= 50 cm^2) and I is the galvanic current.

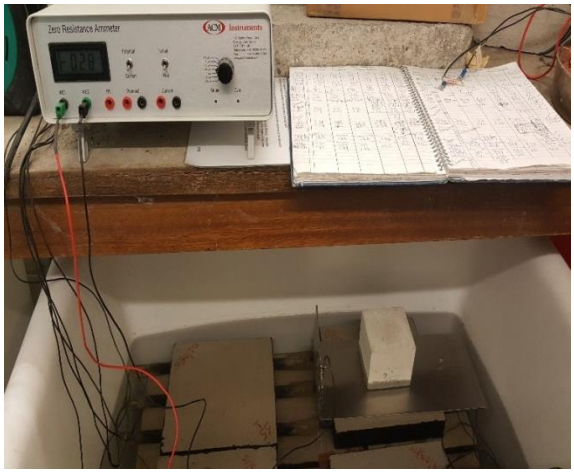

Figure 3: Galvanic current measurement using the Zero Resistance Ammeter (ZRA).

Figure 4: Collection of dry drilled dust samples for analysis

2.3.2 Drilled dust sample analysis

X-ray fluorescence (XRF), X-ray diffraction (XRD) and thermogravimetric analysis (TGA) were performed on dry drilled dust samples collected at depths of 30mm (representing cover) and 65mm from the uncoated surface of the specimen after 1750 days exposure to the regime given in Table 3. Dry drilled dust samples of AACM and PC concrete for bound chloride analysis were collected at depths of 15, 25, 30, 35, 50 and 65mm from the uncoated surface as shown in Fig. 4. Approximately 15 grams of drilled dust samples per each profile depth were collected at depths greater than 5mm from the drilled surface. The chloride analysis were performed in accordance with recognised standards [28, 29].

Chemical compositions of the AACM and PC drilled dust samples were analysed using a wavelength dispersive sequential X-ray fluorescence Philips PW2440 spectrometer. A Philips X-Pert X-ray diffractometer operating with a Cu Kα radiation source (40 KV and 40 mA, wavelength λ=0.154056 nm [6.07 x10^{-9} in.]) was also used to characterize the drilled dust samples. XRD analysis was performed by scanning from 5^0 to 75^0 at an angle of 2Θ; the scan step size was 0.016711 with a counting time step of 0.1 s. Thermogravimetric and differential analysis (TGA) was performed on the drilled dust samples to determine and quantify the

geopolymerization and hydration products using a NETZSCH STA 409 PC/PG device. AACM and PC drilled dust samples were heated up to 1000^0C at a rate of 20^0C/min in nitrogen gas.

2.3.3 Pore solution analysis

The core drilling operation was performed on the AACM and PC concretes after 850 and 1750 days under the exposure regime. Four cores per corrosion specimen of dimensions 50mm diameter by 60 mm depth were drilled in between the embedded steel bars (Fig. 5). Each core was sliced with a masonry saw into three discs at 0-20, 20-40 and 40-60mm depths (Fig. 6). Expression of concrete pore solution was carried out by placing three discs from the same depth, for example 0–20mm depth from the three cores per each concrete mix, into a pore fluid extraction device similar to *Barneyback and Diamond* [30]. The pore solution extraction device with the three discs inside it was placed in a compression testing machine under its loading platen and a compressive load was applied at a steady rate of 10KN/sec. The pore solution was extracted through a suction action without allowing contact with air and stored in plastic vials. The same procedure was repeated on concrete core discs representing 20-40mm and 40-60mm depths (Fig. 6).

Free chloride concentration was determined by dipping a chloride ion selective electrode (ISE) into pore solutions while a double junction pH electrode was used to measure its alkalinity.

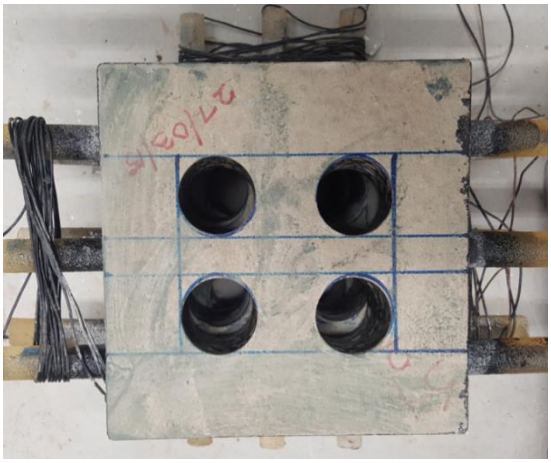

Figure 5: Cores (50mm dia X 60mm depth) drilled in-between embedded steel

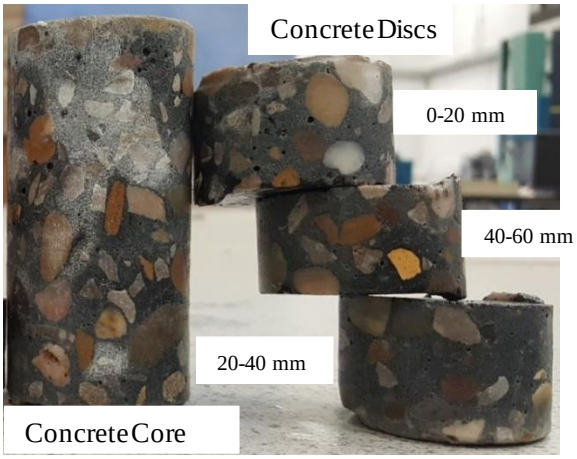

Figure 6: Concrete discs obtained from cores

2.3.4 Corrosion product analysis

The triplicate reinforcement bars embedded in AACM and PC concrete were retrieved after 1750 days exposure to the curing regimes. The extracted triplicate reinforcement and the concrete around their surface were visually examined. The reinforcement was then gently cleaned with acetone to remove all contamination and loose corrosion products.

The surface area and roughness of the cleaned rebars were examined with the aid of an infinite focus variation optical system manufactured by Alicona. 3D scanning in X, Y and Z directions on the steel surfaces containing pitting corrosion was carried out to provide topographical information from the variation of focus.

3.0 EXPERIMENTAL RESULTS AND DISCUSSION

3.1 Concrete characterization

3.1.1 Chemical analysis

X-ray fluorescence results of AACM 1, 2, 3 and PC concrete drilled dust samples taken at 30mm and 65mm depths from the exposed face of the specimen to the chloride solution after 1750 days of chloride exposure are shown in Table 4. The 30mm depth represents the cover to

the steel bars in the concrete. The results show the chemical compounds present in the AACM and PC concrete which influence the initiation and propagation of steel reinforcement corrosion. Table 4 shows the presence of sulfur in both the AACM and PC concrete in SO_3^{2-} oxidation state. Significantly greater amounts of SO_3^{2-} are present in the pore matrix of the AACM concrete than the PC concrete, both at the steel-concrete interface level (30mm depth) and at 65mm depth. For example, SO_3^{2-} contents of AACM 1, 2, 3 and PC concrete at 30mm depth are 0.81%, 0.64%, 0.73% and 0.34% respectively. The corresponding values at 65mm depth are 1.02%, 1.27%, 1.53% and 0.32% respectively. These represent 50% to 80% higher SO_3^{2-} contents in the AACM concrete than the PC concrete. The presence of sulfide in the pore matrix of concrete is known to reduce the redox reaction at the steel concrete interface [8, 12]. Blends of GGBS in concrete mixes can produce aqueous sulfur in the concrete pore solution in various oxidation states such as H_2S, Sn^{2-}, SO_3^{2-}, $S_2O_3^{2-}$ and SO_4^{2-} depending on the content and degree of hydration of the GGBS [31]. The presence of high sulfide content in AACM concrete will create a highly reducing pore solution environment at the steel-concrete interface and help prevent chloride induced corrosion reactions.

The sulfides present in the pore system of AACM concrete form sulfate oxides in the presence of available oxygen, thus reducing the oxygen concentration at the steel-concrete interface [32]. The deprivation of oxygen at the steel concrete interface results in a reducing environment, impeding initiation and propagation of pitting corrosion. MacPhee and Cao [33] suggested that the reducing environment caused by the high sulfide concentration will favour formation of Fe^{II} rather than Fe^{III}, which is associated with the αFe_2O_3 layer on the steel surface. In the process, precipitates of Mackinawite ($Fe_{1+X}S$) are formed on the steel surface rather than an iron oxide passive film [34]. The depletion of oxygen concentration in AACM concrete due to a high concentration of sulfide affects the development of a protective passive layer on the steel

surface since oxygen concentration is required for the cathodic reaction which produces these passive films in OPC concrete [32]. This aspect requires further research.

The data in Table 4 show that except Ca^{2+} the other alkalis Na^{+}, K^{+}, Al^{3+} and Mg^{2+} are more abundant in AACM than PC concrete. For example, the sum of these alkalis at 30mm depth in AACM 1,2,3 and PC concrete is 14.4%, 14.86%, 18.17% and 5.07% respectively. These alkalis contribute to the high alkalinity of AACM concrete, which also provides corrosion resistance to steel reinforcement. The effect of these alkalis on the corrosion resistance of steel reinforcement is discussed in Section 3.3.

Table 4: Chemical composition of AACM and PC drilled powder samples at 30 and 65mm depth after 1750 days curing regime

		30mm depth (%)				65mm depth (%)			
Element	Compound	AACM 1	AACM 2	AACM 3	PC	AACM 1	AACM 2	AACM 3	PC
Na	Na_2O	2.83	2.83	2.55		3.67	4.55	4.73	0.45
Mg	MgO	3.11	2.99	3.85	0.70	2.07	3.00	2.68	1.37
Al	Al_2O_3	7.84	8.12	10.56	3.55	6.90	7.08	8.77	6.10
Si	SiO_2	48.49	42.72	31.98	74.96	54.50	47.97	40.70	54.41
S	SO_3	0.81	0.64	0.73	0.34	1.02	1.27	1.53	0.32
K	K_2O	0.62	0.92	1.21	0.82	0.90	0.89	1.05	1.39
Ca	CaO	34.33	39.08	46.21	15.78	28.61	33.56	38.81	29.66
Ti	TiO_2	0.20	0.29	0.30	0.07	0.51	0.30	0.15	0.17
Fe	Fe_2O_3	0.89	1.14	1.27	3.05	1.27	0.99	1.17	4.92
Sr	SrO	0.028	0.04	0.05	0.04	-	0.07	0.07	0.06
P	P_2O_5	0.08	0.14	-	0.10	0.08	-	-	0.68
Mn	MnO	0.23	0.44	0.39	-	0.32	0.33	0.34	-
Zn	ZnO	0.27	0.65	0.62	-	-	-	-	-
Cl	Cl	0.28	0.29	0.31	0.60	0.17	0.23	0.25	0.48

3.1.2 Mineralogical analysis

Figure 7a. shows the X-ray diffraction (XRD) results of AACM drilled dust at 30mm depth (cover to reinforcement), after 1750 days of exposure to an environment capable of initiating chloride induced corrosion. The results show the presence of quartz, calcite, halite, augite,

cordierite and gypsum in the AACM concrete drilled dust samples. Figure 7b for PC concrete drilled dust samples shows the presence of quartz, calcite, Portlandite, hydrotalcite, anatase, ettringite, Friedel's salt and hematite. The mineralogical compositions of AACM and PC concretes have a critical effect on their chloride binding capacity, porosity and alkalinity, each of which is responsible for the corrosion behaviour of both concretes.

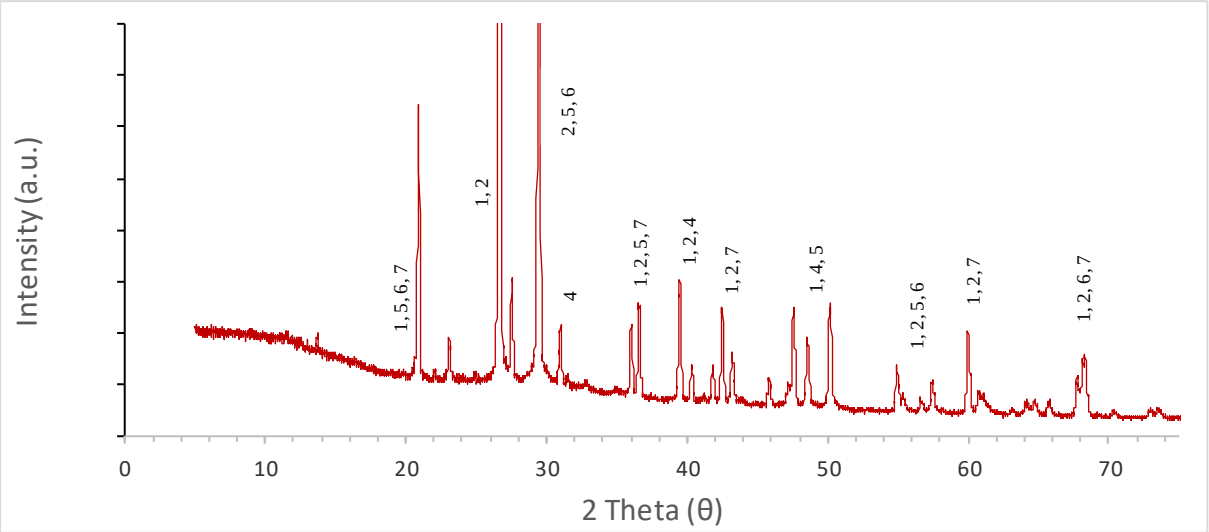

Figure 7a: XRD of AACM drilled dust samples at steel concrete interface after 1750 days exposure period

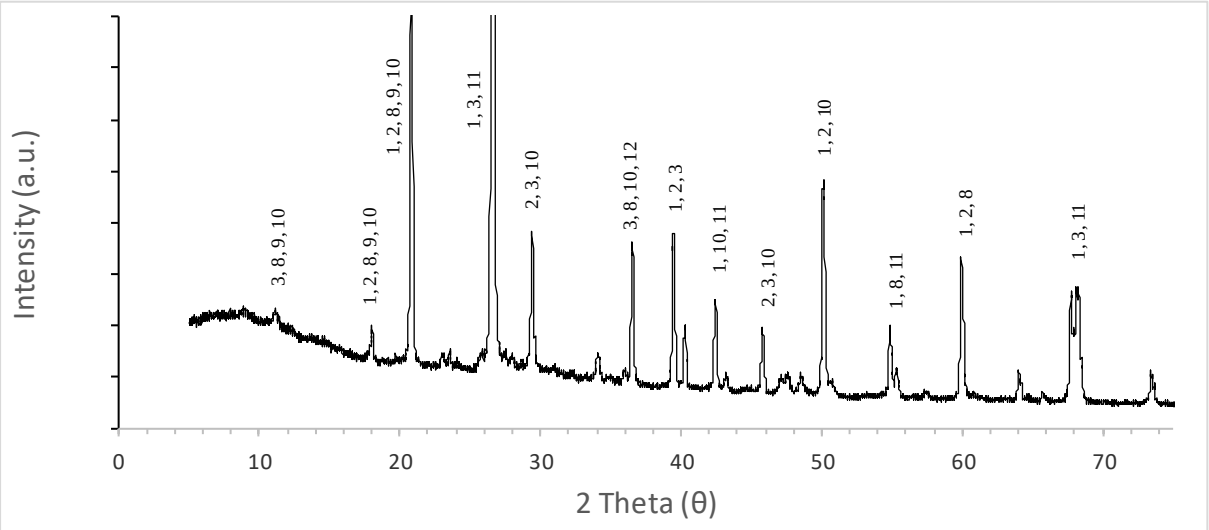

Figure 7b: XRD of PC drilled dust samples at steel concrete interface after 1750 days exposure period

Legend

		AACM 3 (%)	PC (%)
1	Quartz	57	44
2	Calcite	20	15
3	Portlandite	-	5
4	Halite	4	-
5	Augite	7	-
6	Cordierite	8	-
7	Gypsum	4	-
8	Hydrotalcite	-	3
9	Anatase	-	1
10	Ettringite	-	2
11	Friedel's salt	-	30
12	Hematite	-	1

The higher content of quartz in AACM concrete (57%) than PC concrete (44%) accounts for its higher percentage of solid gel and, therefore, lower porosity than PC concrete [16]. The porosity of AACM 1 is 4.64%, 6.53% and 9.90% compared with 14.02%, 13.30% and 17.43% for PC concrete after 28 days curing under wet/dry, wet and dry curing, respectively. The corresponding values for AACM 2 are 6.67%, 8.02% and 10.70% while for AACM 3 they are 7.71%, 9.05% and 11.93% [16]. Hence, fewer chloride ions diffuse through the pore matrix of AACM concrete relative to PC concrete [35], which will influence chloride induced corrosion of embedded steel.

It is also observed that the chloride binding capacity which regulates the amount of free chloride available to support corrosion is lower in AACM than PC concrete [23]. Hence, a higher amount of free chloride is released in the pore matrix of AACM concrete. The higher chloride binding capacity (acid and water soluble) of PC concrete [23] is due to the significant presence of hydrotalcite and Friedel's salts (Fig. 7b). These compounds are absent in the AACM while relatively small amounts of halite and gypsum provide chloride binding in AACM concrete (Fig. 7a). Phases such as hydrotalcite provide surface absorption to physically

bind chloride and are sensitive to changes in pH, chloride concentration and total ionic strength [36]. The C_3A content in PC concrete produces $Ca_6Al_2O_6.CaCl_2.10H_2O$ (Friedel's salt) which accounts for its high chloride binding capacity [23]. The presence of gypsum in AACM concrete increases solubility of ions leading to the release of sulfate ions into its pore solution [15]. Halite is soluble in water and releases chloride into the pore fluid [37].

The alkalinity of concrete at the steel interface is important for preserving its passivity. The percentage of calcite in both AACM (20%) and PC concrete (15%), as shown in Figure 7a and 7b, relates to the degree of carbonation which causes a reduction in the pore solution alkalinity. Hydroxyl ions (OH-) within the pore solution are displaced by carbonation thereby depleting the protective passive film around the reinforcing steel. Portlandite which is only present in PC concrete (5%) serves as a booster for pore solution alkalinity by replacing the (OH-) consumed during the carbonation process. The carbonated AACM concrete does not contain Portlandite, however, it has higher contents of alkalis Na^+, Al^{3+} and Mg^{2+} than PC concrete, Table 4[38]. These alkalis contribute significantly to the alkalinity of pore fluid in AACM concrete [38]. Common atmospheric rust, hematite (1%), which is present in only PC concrete will support the corrosion of embedded steel [39].

3.1.3 Thermogravimetric analysis

Figure 8a shows the derivatives of thermogravimetry (DTG) and thermogravimetry (TG) analysis of AACM and PC drilled dust samples collected at 30mm depth (cover to steel), which is heated from 33^0C to 1000^0C. Thermogravimetry (TG) analysis of the concrete drilled dust samples collected at the cover depth shows the decomposition of chemical compounds which affect steel corrosion, such as hydrotalcite and calcite in AACM concrete and Friedel's salt, Portlandite and calcite in PC concrete. It validates the chemical and mineralogical analysis results.

Three dominant peaks were observed due to interlayer water molecule (H_2O) released between 33^{0}C to 250^{0}C, hydroxyl (OH-) released between 350^{0}C to 480^{0}C and carbonate ions released between 680^{0}C to 860^{0}C as shown in Fig. 8a and 8b. The first peaks at 33^{0}C to 250^{0}C relates to the bound water, dehydration of C-S-H, ettringite (AFt) and monosulfoaluminate (AFm) [40, 41].

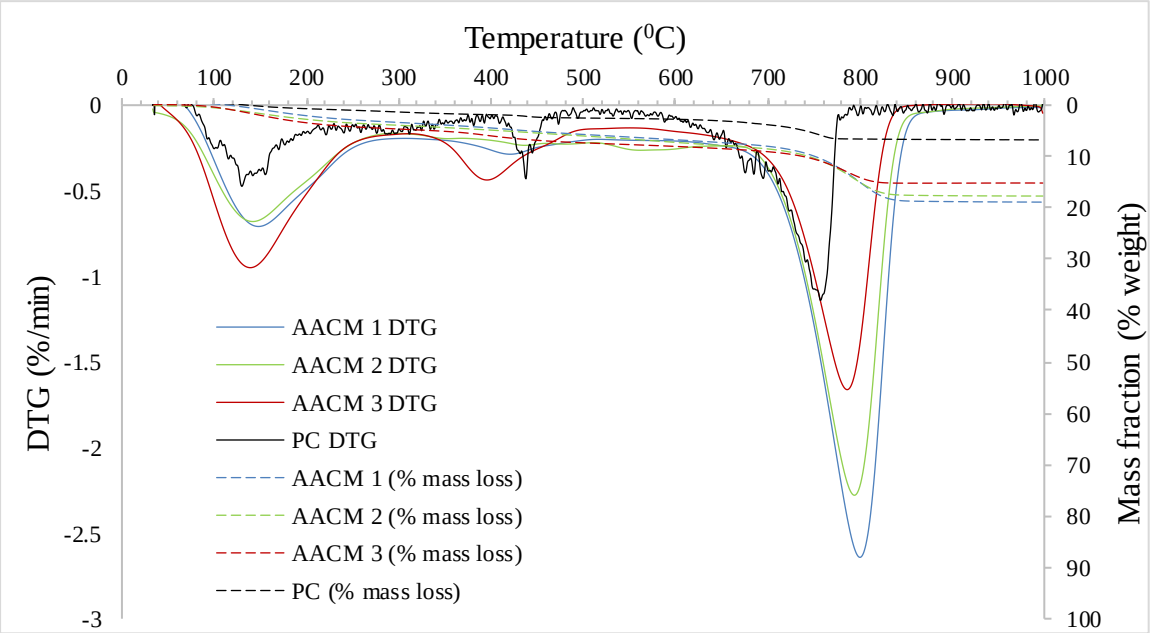

Figure 8a: DTG-TG curves of AACM and PC concrete

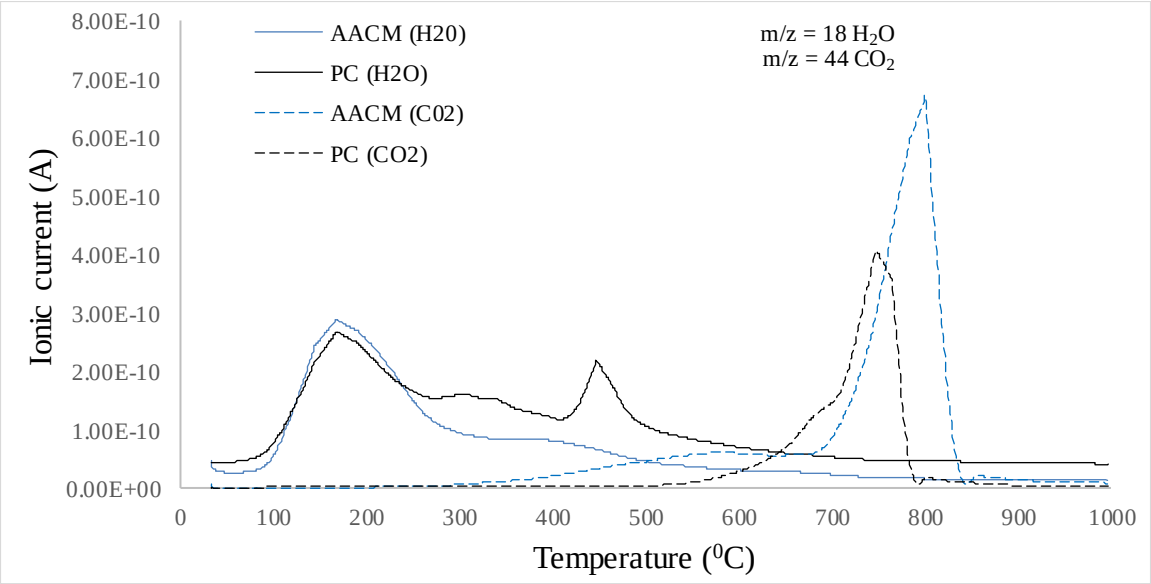

Figure 8b: Recrystallized H_2O (m/z = 18) and CO_2 (m/z = 44) for AACM and PC concrete

The intensity of the first peak is greater in AACM than PC concrete mainly due to its high volume of C-S-H, which is consistent with the XRD result. The presence of ettringite and gypsum in PC concrete resulted in its lower first peak than AACM concrete. The bonding of water molecules at the interlayer of these compounds is through H-bonding [36, 42] which also affects chloride concentration. Previous research [23] has revealed higher physically bound chloride in AACM concrete than PC concrete due to the likelihood of an ordered structure of H-bonding of the water molecules at the interlayers of C-S-H in AACM concrete.

The second dominant peak at 350^0C to 480^0C in Fig 8a represents the decomposition of Portlandite and hydrotalcite in PC concrete, which releases hydroxyl ions. XRD analysis show the presence of Portlandite and hydrotalcite in PC concrete, while they are not traceable in AACM concrete. The third dominant peak was observed at 680^0C to 860^0C in AACM and PC concrete as shown in Figures 8a and 8b. The peak intensity was greater in AACM concrete due to the higher amount of calcite (20%) as shown in Fig. 7a compared with 15% calcite in PC concrete. Decarbonation of the calcite at 680^0C to 860^0C released CO_2.

3.2 Electrochemical monitoring

3.2.1 Corrosion potential E_{corr}

The electrochemical corrosion potential E_{corr} readings of AACM concrete specimens up to 1750 days under corrosion inducing exposure (Table 3) are presented in Figure 9. However, E_{corr} data for PC concrete in Fig 9 represent 1580 days exposure due to a 170 days' delay in producing the PC concrete specimens. The specimens were exposed to the following environments (Table 3) in sequence to support accelerated corrosion by providing high levels of chloride and oxygen at the steel surface: 1. Immersion in 5% chloride solution at $20 + 2^0$C in accordance with standards [28, 29]; 2. Dry curing at $20 + 2^0$C and 65% R.H.; 3. Environment

chamber at 50^{0}C and 75% R.H; 4. 1 day wet 20 + 2^{0}C followed by 6 days dry curing cycles; 5. Wet curing at 40^{0}C.

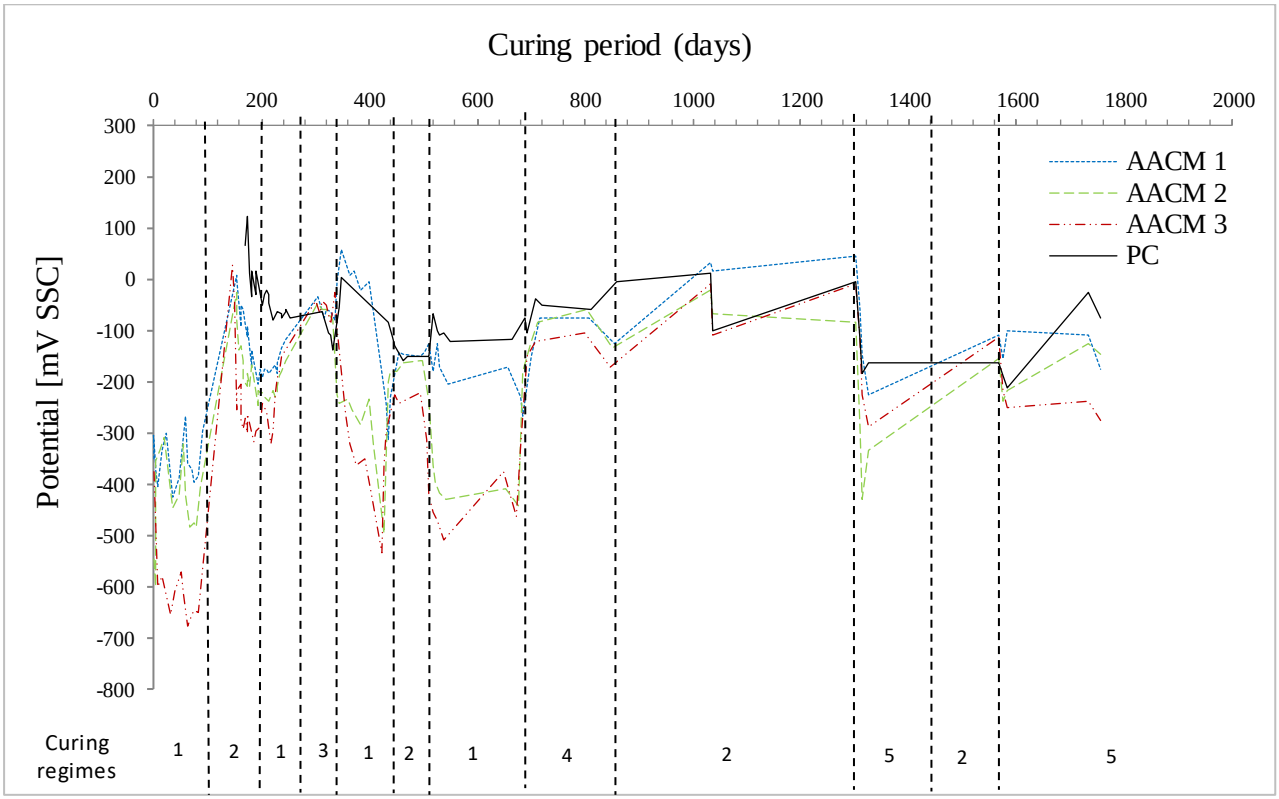

Figure 9: Corrosion potential E_{corr} in AACM 1, 2, 3 upto 1750 days exposure and PC concrete for 1580 days exposure (due to 170 days' delayed start).

Legend of curing regimes

1 Chloride diffusion (20 + 2^{0}C)
2 Dry curing (20 + 2^{0}C and 65% R.H.)
3 Environmental chamber (50^{0}C, 75% R.H.)
4 1 day wet/6 days dry curing cycle
5 Wet curing (40^{0}C)

AACM 1, 2 and 3 corrosion specimens were subjected to four cycles of chloride diffusion exposure at ages of 0 - 90, 190 - 260, 340 - 440 and 510 - 690 days while PC concrete specimens were exposed to three cycles at ages of 190 - 260, 340 - 440 and 510 - 690 days, omitting the first chloride cycle and most of the second dry curing cycle.

The corrosion potentials E_{corr} in AACM concrete reached maximum negative values during cycles 1 and 5 (Figure 9) which represent total submersion in the chloride solution or pure water

respectively. The values reach as low as -677 mV during the first cycle (0 -90 days) of exposure (Fig. 9). The corresponding Ecorr values in the control PC under the same submerged exposure are above -200 mV which indicates a passive state of the steel (Fig. 9). The steel bars in AACM 1 and 2 concrete which reached potentials as low as - 677mV do not show signs of chloride induced corrosion as shown in Fig. 14 (section 3.4) during inspection of the steel surface after 1750 days of exposure. AACM 3 shows some signs of corrosion but much less than the PC concrete sample.

The very negative E_{corr} values in AACM concrete are attributed to the depletion of oxygen concentration at the steel-concrete interface preventing the passivation of the embedded steel. Factors affecting the onset of chloride induced corrosion in AACMs include mix design, curing environment, pore solution chemistry and more importantly the redox environment near the steel interface [8, 12, 18]. The presence of sulfides in AACM concrete (Table 4) causes a highly reducing redox environment which depends on the GGBS content and the degree of reaction [8, 32]. Sulfur content in the GGBS binder from various oxides such as H_2S, Sn^{2-}, SO_3^{2-}, $S_2O_3^{2-}$ and SO_4^{2-} leads to a decrease in dissolved oxygen concentration in the pore solution of AACMs [31]. Table 4 shows a significant amount of SO_3 at the steel interface of AACMs, which reduces the amount of dissolved oxygen within their pore matrix, therefore, resulting in a very negative E_{corr} value of -677 mV. Similar E_{corr} values between -450 mV to -600 mV, without showing signs of corrosion, were observed for steel bars immersed in NaOH solutions of 0.8M, 1.12M and 1.36M simulating pore solution of low calcium alkali activated concrete [5]. Steel reinforced alkali activated slag containing 0 to 8% by weight of NaCl added as admixture and cured at 90% R.H for 100 days also showed similar results [43].

The formation of sulfides in the AACM matrix around the steel interface affect the redox environment by depleting the availability of oxygen required to support corrosion. This induces a more negative potential, $E_{corr,}$ in specimens submerged in the chloride solution and water which also provide a low oxygen environment. A significant shift towards a more positive E_{corr} value is observed when the AACM concrete becomes partially saturated under curing type 2: dry curing at 20 + 2^{0}C and 65% R.H.(Fig. 9), curing type 3: environment chamber at 50^{0}C and 75% R.H. and curing type 4: 1 day wet followed by 6 days dry curing cycles. This is due to sufficient oxygen becoming available at the steel-concrete interface to support an oxidizing environment during partial saturation of AACM concrete. For example, in Fig. 9, AACM 3 concrete shows a sharp increase in E_{corr} from -677 to +50mV during change over from chloride solution curing (cycle 1, 0 - 90 days) to dry curing (cycle 2, 90 - 190 days). A similar drop in corrosion potential of AACM 3 concrete is also observed when moving from the environment chamber at 50^{0}C and 75% R.H (curing cycle 3, Fig.9) to the submerged chloride solution curing cycle 1.

The control PC concrete does not show significant variation of E_{corr} when exposed under the different curing environments (Fig.9). The values ranged between 0mV and -250mV, indicating a non-corrosive state according to E_{corr} values given in the literature [26]. However, the images of split specimens in Fig. 14, after 1750 days of exposure show significant pitting corrosion of steel in PC concrete. The E_{corr} values of AACM concrete are highly affected by the saturated state of the matrix and lack sufficient stability under cyclic wet-dry exposure to provide a reliable corrosion indicator for the steel. However, the E_{corr} values of the AACMs are fairly stable (0 to -250 mV) during the prolonged partially saturated exposure period from 660 to 1300 days in Figure 9.

Bastidas et al. [44] studied the passive state stability of steel embedded in alkali activated fly ash mortars. The fly ash reinforced mortar was cured for 94 days at 95% R.H. followed by 150 days in laboratory air and then 220 days at 95% R.H. The corrosion potential E_{corr} decreases by 400 mV when moved from partial to complete saturated environment. The authors [44] attributed the low resistivity of fly ash mortar to the degree of saturation within its pore matrix, shifting the E_{corr} value to a more negative potential when placed in a completely saturated environment. Other researchers have attributed the negative shift in E_{corr} in fly ash mortar to insufficient oxygen at the steel concrete interface which is not taken into account by the digital voltmeter (DVM) [45, 46]. Care must, therefore, be taken when interpreting the results of E_{corr} in AACM concrete under different curing regimes.

Unlike alkali activated slag concrete, steel embedded in alkali activated fly ash concrete has a low sulfide content similar to PC concrete and its passivation mechanism is also similar due to identical oxidizing capacities of the pore solution [8]. The E_{corr} values recorded for alkali activated fly ash concrete are between 0 mV to -200 mV [47]. In some cases the E_{corr} value for alkali activated fly ash is lower than a comparative PC concrete, which is attributed to the inhibitive properties of soluble silicates in its pore solution [8]. The presence of sulfides in the pore solution of alkali activated slag dominates the inhibitive properties of soluble silicates, which will have a salient effect on the redox potential at steel concrete interface as evident in Figure 9.

3.2.2 Corrosion current density I_{corr}

The corrosion current density I_{corr} in AACM 1, 2, 3 and PC concrete was measured using a zero-resistance ammeter ZRA. It provides the basis for determining the severity of corrosion of the steel bars in the concrete. The values of I_{corr} are plotted against exposure period in Fig.

10. The measurements were taken up to 860 days exposure under different curing regimes presented in Table 3 and Fig.10.

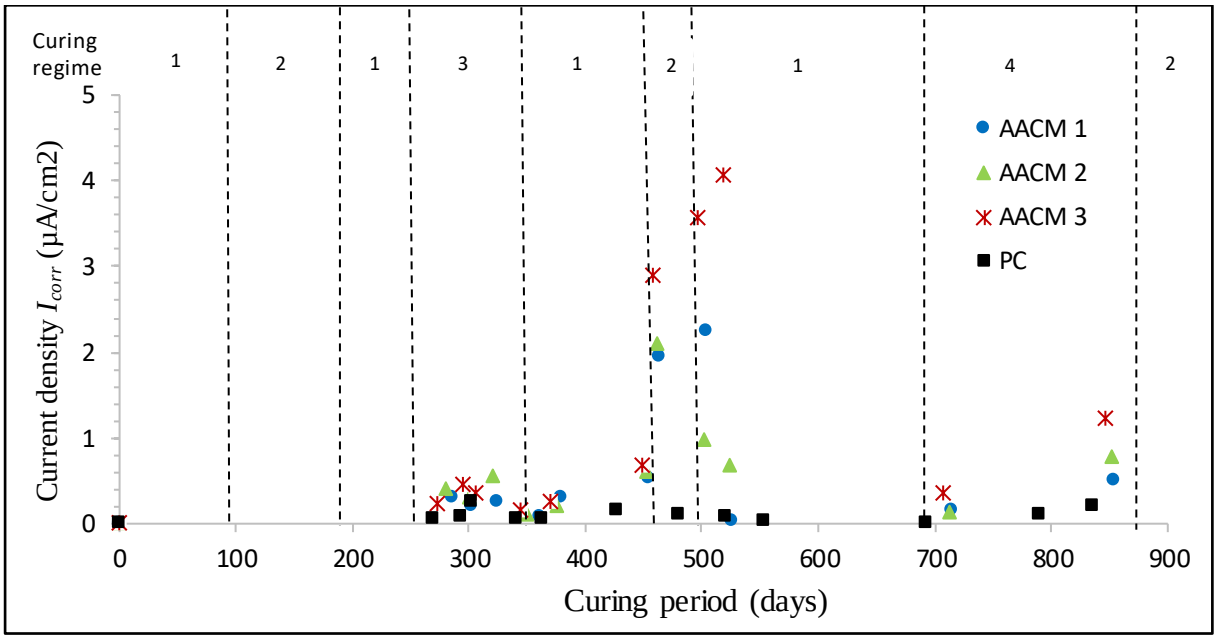

Figure 10: Current density I_{corr} in AACM 1, 2, 3 and PC concrete up to 860 days exposure

Legend of curing regimes
1 Chloride diffusion (20 + 2^{0}C)
2 Dry curing (20 + 2^{0}C and 65% R.H.)
3 Environmental chamber (50^{0}C, 75% R.H.)
4 1 day wet/6 days dry curing cycle

The corrosion current density I_{corr} in AACM is higher than in PC concrete as shown in Fig. 10. The I_{corr} in AACM concrete is relatively low from 290 days to 450 days before showing high peak values when it encounters exposure 2 (dry curing). AACM 3 has the highest I_{corr} value of 4.06 µA/cm^2 at 520 days exposure, followed by AACM 1 and 2 with I_{corr} values of 2.26 and 2.1 µA/cm^2 respectively. The reduction in molarity (concentration) of the activator increases the I_{corr}. By comparison, the I_{corr} values of the control PC concrete remain fairly stable with a maximum of 0.26 µA/cm^2 at 300 days exposure, which suggests a passive state of steel. However, steel embedded in AACM 1 and 2 concrete shows little sign of active corrosion after 1750 days exposure as shown in Fig. 14 (section 3.4) unlike PC concrete that shows the greatest

degree of pitting corrosion. The process of chloride induced corrosion is anodically controlled [48] which requires a corresponding cathodic reaction to sustain the dissolution of negatively charged electrons of iron into the electrolyte (pore solution) at the anodic site. The cathode provides the reaction of oxygen with the negatively charged electrons. However, the depletion of oxygen in AACM concrete at the steel surface due to the formation of sulfides in the matrix stifles the cathodic reaction and hence the corrosion process.

The high I_{corr} values between 450 to 550 days (during curing cycle 1 and 2) exposure in Fig. 10 relates to oxidation of sulfide during the partially dry curing state of AACM concrete (Table 3) rather than an increase in the anodic reactant (chloride concentration) at the steel surface. The change over from the submerged state (cycle 1) to the dry curing state (cycle 2) increased the oxygen concentration required for the cathodic reaction as well as the oxidation of the sulfide, thus producing elemental sulfur deposits on the steel surface embedded in AACM concrete as seen in Fig. 15. *Holloway and Sykes* [43] observed similarly high shifts in the I_{corr} of slag cement mortar and attributed it to the depletion of the cathodic reactant (oxygen) rather than initiation of pitting corrosion. Sulfur deposits are formed at the cathodic site by the oxidation of hydrogen sulfide in the pore solution as seen in Fig 15. The inhibition of the cathodic reaction produces higher I_{corr} and more negative E_{corr} values in non-corroding steel as seen for AACMs in Figs 9 and 10. The stifling of anodic reactions results in lower I_{corr} and a less negative E_{corr} values[43] as observed for PC concrete in Figs 9 and 10.

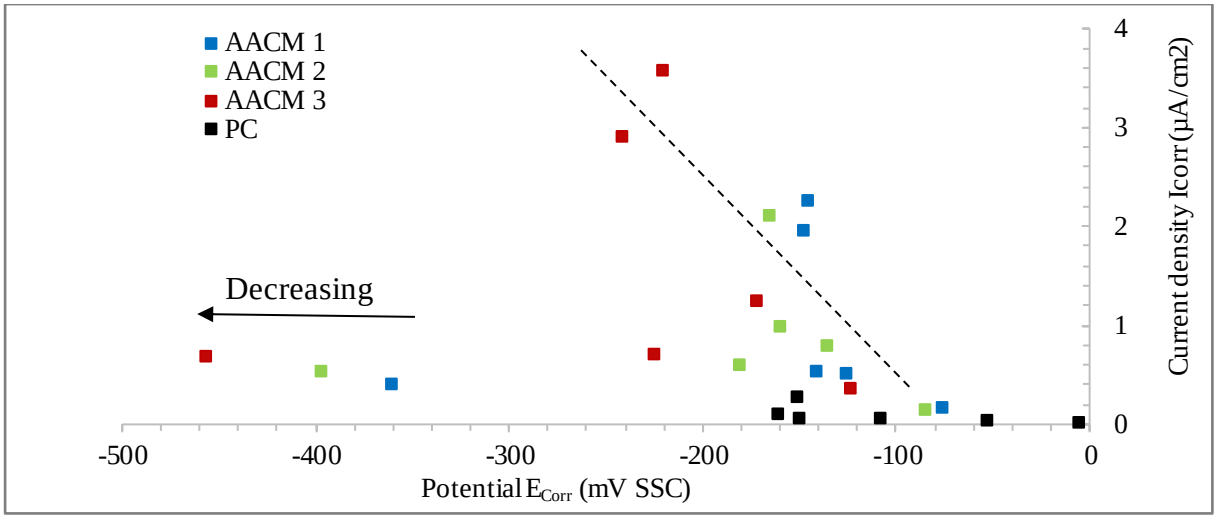

Figure 11: Anodic polarization of steel reinforcement embedded in AACM and PC concrete

The relationship between I_{corr} and the anodic polarization (E_{corr}) of steel embedded in AACM and PC concrete is shown in Fig. 11. Increasing values of I_{corr} are observed at decreasing E_{corr} up to about -250 mV in AACM concrete. A steep linear relationship between I_{corr} and E_{corr} is observed between about -150 to -250 mV which indicates anodic controlled corrosion in partially saturated AACM concrete. Thereafter, low I_{corr} values occur at more negative E_{corr} values of under -360 mV in AACM concrete. *Holloway and Sykes* [43] observed a similar corrosion mechanism showing high I_{corr} peaks at less negative E_{corr} values than -200 mV, while I_{corr} values were lowest at a more negative E_{corr} value of -800 mV for steel embedded in alkali activated slag. *Mundra et al* [5] observed peak I_{corr} value at E_{corr} under -700 mV and the lowest I_{corr} value at -1100 mV for steel bars in simulated pore solutions of alkali activated concrete. The two extreme I_{corr} values (high peak and lowest) signify the anodic and cathodic current peaks respectively. The anodic current peak indicates oxidation of Fe^{2+} to Fe^{3+} species [5] forming a passive film on steel surface containing polymorphs of either FeOOH or Fe_2O_3. There is inconclusive information in literature on the various polymorphs of either FeOOH or Fe_2O_3 formed by the oxidation product of Fe^{3+} species [5, 49, 50].

In this study, the anodic current peak at -220 mV for AACM 3 relates to it being completely saturated during curing cycle 1 (Table 3), with sulfides, HS^-, within its pore matrix hindering the formation of a passive film on the steel surface. There is competitive adsorption between HS^- and OH^- at the active sites on the steel surface. The absorbed HS^- leads to the formation of a colloidal suspension of $NaFeS_2$ (complex of Fe^{3+}) and subsequently breaking down of the passive film at higher potentials [43]. The cathodic current peak at -450 mV for AACM 3 concrete relates to its partially saturated state during cycle 2 (dry) curing (Table 3) when oxygen availability results in the oxidation of sulfide to form elemental sulfur deposits on the pores of the passive film [5, 43]. The passive film which was depleted during the anodic current peak is, therefore, repaired during the cathodic current peak [5].

3.3 Chloride contents and alkalinity of pore solution

3.3.1 Free chloride

Table 5 shows the free chloride concentrations, hydroxyl concentration, Cl^-/OH^- ratios and bound chloride (acid soluble) of AACM and PC concrete at 180, 270, 540, 860 and 1750 days exposure.

Table 5: Free chloride and hydroxyl concentration in AACM and PC concrete at different ages of exposure

Exposure (days)	mix	Free Cl^- (mol/L)			OH^- (mol/L)			Cl^-/OH^-			Acid Cl^- (%wt. of binder)		
		Depth (mm)											
		10	30	50	10	30	50	10	30	50	10	30	50
180	AACM 1	0.011	0.006	0.002	0.155	0.347	0.363	0.07	0.02	0.01	0.39	0.04	0.04
	AACM 2	0.015	0.008	0.003	0.204	0.316	0.363	0.07	0.03	0.01	0.47	0.04	0.04
	AACM 3	0.018	0.010	0.004	0.129	0.257	0.288	0.14	0.04	0.01	0.24	0.22	0.04
	PC	0.010	0.005	0.002	0.014	0.058	0.074	0.71	0.09	0.03	0.99	0.66	0.17
270	AACM 1	0.020	0.017	0.012	0.125	0.317	0.333	0.16	0.05	0.04	0.60	0.35	0.06
	AACM 2	0.023	0.017	0.014	0.174	0.286	0.333	0.13	0.06	0.04	0.62	0.37	0.06
	AACM 3	0.025	0.018	0.014	0.099	0.227	0.258	0.25	0.08	0.05	0.77	0.53	0.14
	PC	0.022	0.013	0.008	0.011	0.028	0.044	2	0.46	0.18	2.4	1.11	0.07
540	AACM 1	0.036	0.023	0.016	0.046	0.061	0.011	0.78	0.38	1.48	-	-	-

	AACM 2	0.058	0.036	0.024	0.055	0.078	0.015	1.05	0.46	1.63	-	-	-
	AACM 3	0.071	0.056	0.031	0.078	0.093	0.019	0.91	0.6	1.66	-	-	-
	PC	0.032	0.018	0.012	0.016	0.023	0.036	2.06	0.78	0.33	-	-	-
860	AACM 1	0.043	0.033	0.028	0.013	0.018	0.027	3.27	1.82	1.05	-	-	-
	AACM 2	0.061	0.040	0.039	0.015	0.019	0.028	4.09	2.1	1.38	-	-	-
	AACM 3	0.067	0.059	0.052	0.015	0.021	0.031	4.47	2.81	1.67	-	-	-
	PC	0.022	0.014	0.018	0.008	0.013	0.023	2.76	1.08	0.78	-	-	-
1750	AACM 1	0.041	0.034	0.027	0.017	0.02	0.032	2.43	1.71	0.84	0.54	0.27	0.05
	AACM 2	0.059	0.046	0.035	0.023	0.022	0.036	2.55	2.1	0.97	0.63	0.36	0.09
	AACM 3	0.070	0.06	0.051	0.026	0.025	0.033	2.69	2.4	1.53	0.82	0.45	0.18
	PC	0.022	0.014	0.008	0.009	0.014	0.022	2.43	1.02	0.36	3.25	3.07	2.54

Portland cement concrete has lower concentrations of free chloride than AACM concrete. For example, the free chloride concentrations in PC concrete are 0.005 and 0.014 mol/L at 30mm depth after 180 and 1750 days exposure respectively. The corresponding values are 0.006 and 0.034mol/L for AACM 1, 0.008 and 0.046mol/L for AACM 2 and 0.010 and 0.060 mol/L for AACM 3. The lower concentration of free chloride in the pore solution of PC concrete is predominantly influenced by its greater chloride binding capacity [2, 4] which increases its acid soluble chloride content as shown in Table 5. Conventional PC concrete has higher binding capacity due to the presence of C_3A and C_4AF in its binder (Table 2). The unhydrated portion of aluminate (C_3A) and aluminoferrite (C_4AF) of PC binders reacts with the chloride ions in the pore solution during the chloride exposure period, forming Friedel's salt ($Ca_6Al_2O_6.CaCl_2.10H_2O$) and calcium chloroferrite [51]. The lack of calcium aluminate (C_3A) and aluminoferrite (C_4AF) in the AACM concrete (Fig. 7a) results in its low chloride binding capacity. The chloride binding capacity regulates the amount of free chlorides [22] which initiate reinforcement corrosion when their threshold limits are exceeded.

The acid soluble chloride concentration of the AACM 1, 2 and 3 mixes at 270 days exposure ranges between 0.35 and 0.53 at 30 mm depth (Table 5). However, the longest chloride exposure period occurs between 340 and 690 days (Figure 9) involving chloride diffusion and

capillary absorption due to the intermediate dry exposure period. Therefore, at 690 days of exposure the acid soluble chloride concentrations would have considerably exceeded the permissible level for corrosion initiation of 0.40% by weight of cement which is stipulated in standards for PC concrete [22]. However, corrosion in AACM concrete is controlled by its free chloride in the pore fluid and an acid soluble chloride threshold is therefore not applicable [35]. The free chloride concentrations in AACM and PC concrete show a steady increase up to 860 days exposure with little further increase at 1750 days exposure, as shown in Table 5. The free chloride ingress relates to the exposure regimes presented in Table 3. The alternate exposure in the chloride solution and drying had stopped before 860 days, which was followed by a chloride-free exposure in water (regime 5) or in air (regime 2) up to 1750 days. High chloride ingress occurred in concrete up to 860 days due to both the diffusion and capillary absorption of chloride ions occurring simultaneously when concrete was exposed to cyclic wetting and drying [2, 52]. There is insignificant depletion of the free chloride concentration in both AACM and PC concrete between 860 and 1750 days due to the release of physically bound chloride into their pore solution [23, 35].

The ingress of chloride from the curing environment and leaching of hydroxyl ions from the concrete pore solution occurs by diffusion in saturated concrete and by capillary absorption in unsaturated AACM and PC concretes exposed to wet and dry cycles.

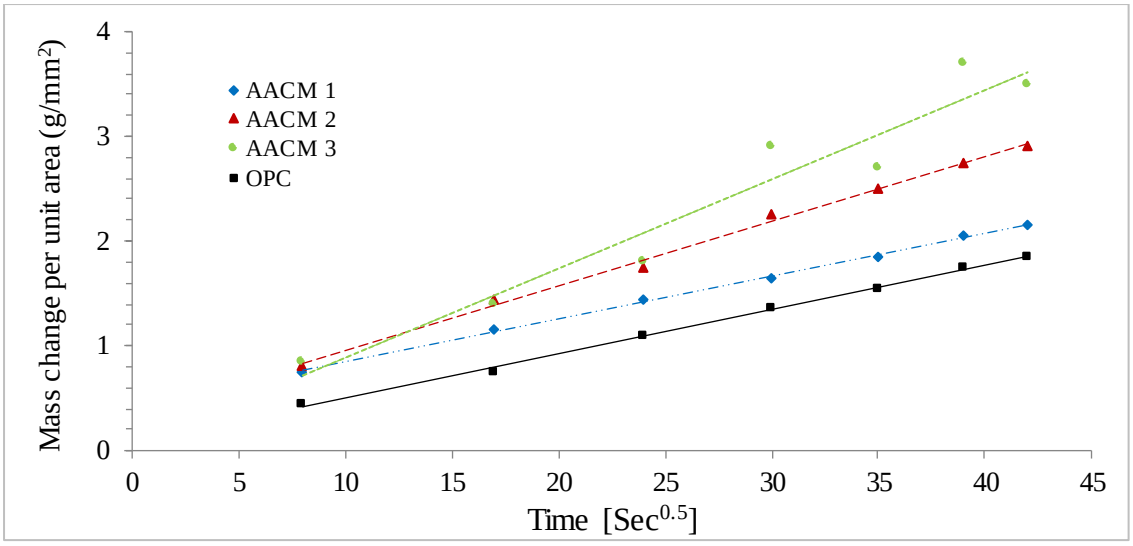

Figure 12: Capillary absorption in AACM 1, 2, 3 and PC concrete.

Figure 12 shows that the capillary absorption in AACM concrete is higher than PC concrete, particularly AACM 3 concrete which shows sorptivity of 0.085 mm/sec$^{0.5}$ compared with 0.042 mm/sec$^{0.5}$ in PC concrete. The higher capillary absorption in AACM concrete relates to its higher volume of large capillary pores (0.01 to 10 µm) than PC concrete [16]. The volume of capillary pores is highest in the AACM 3 concrete [16], which gives it the greatest sorptivity value. However, the total porosity of the AACM 1, 2 and 3 concrete is less than PC concrete, which reduces their chloride diffusion (17).

3.3.2 Hydroxyl concentration

AACM concrete has a higher concentration of hydroxyl ions than the control PC concrete (Table 5). For example, the hydroxyl concentration at 30mm depth is 0.032, 0.036, 0.033 and 0.022 mol/L for AACM 1, 2, 3 and PC concrete respectively at 1750 days exposure. The pore solution alkalinity, therefore, is higher in AACM than PC concrete when subjected to diffusion and capillary absorption of chloride over a long period. The alkalinity in PC concrete is supplied by the hydration product $Ca(OH)_2$ which releases hydroxyl ions (OH-) into its pore solution whereas in AACM concrete it is supplied by the hydroxyl ion concentration of the alkali

activator. This is evident by the highest concentration of hydroxyl ions in AACM 1 concrete (Table 5) which has the highest activator concentration (molarity) (Table 1).

The leaching of hydroxyl ions into the curing solution is more significant in AACM than PC concrete. For example, the hydroxyl concentration at 10mm depth in AACM 1 concrete reduced from 0.155 to 0.017mol/L between 180 to 1750 days exposure. The corresponding values for PC concrete are 0.014 to 0.009 mol/L (Table 5). The alkalinity in PC concrete is relatively stable because of the buffering effect of $Ca(OH)_2$ which releases hydroxyl ions into the pore solution, maintaining the level [12]. This mechanism is not present in AACM concrete. High carbonation in AACM concrete (20% calcite) as shown in the XRD result (Fig. 7a) also plays a significant role in the reduction of pore solution alkalinity compared with PC concrete which has 15% calcite (Fig. 7b).

3.3.3 Chloride/hydroxyl (Cl^-/OH^-) ratio

Figure 13 shows the plot of log (Cl^-/OH^-) at the steel interface (30mm depth) versus exposure time for the AACMs and PC concrete. The Cl^-/OH^- for AACM concretes increases linearly with time up to 860 days of exposure to chloride and dry cycles and remains constant thereafter when further chloride ingress stops due to chloride-free curing cycles (Table 3).

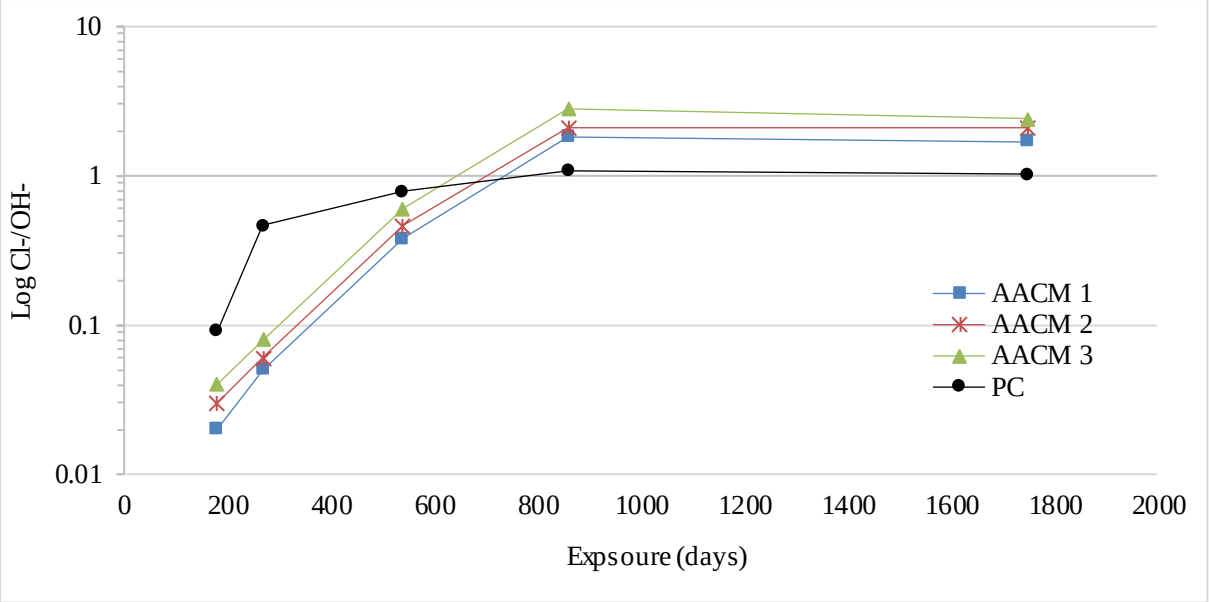

Figure 13: Relationship between log Cl^-/OH^- at steel-concrete interface (30mm depth) and exposure period (Cl/OH threshold for PC is 1 and AACM is 2.8).

PC concrete has higher Cl^-/OH^- ratios than AACM concrete up to 540 days exposure and then a reversed trend is observed. This is characterised by the steep rise in the Cl^-/OH^- ratio up to 270 days followed by small increase. The high chloride binding capacity and buffering effect on OH^- concentration in PC concrete played an important role in the minimal increase of Cl^-/OH^- ratio after 270 days exposure [23]. Chloride ions removed from the pore solution of PC concrete by chloride binding are simultaneously replaced by OH^- through the buffering effect of the hydration product $Ca(OH)_2$, thereby limiting absorption sites for further chloride ingress. There is no similar buffering effect in AACM concrete (Fig. 7a). The critical (maximum) levels of free chloride and Cl^-/OH^- occur at 860 days and remain fairly constant at 1750 days. The Cl^-/OH^- ratios for AACM 1, 2, 3 and PC concrete are 1.82, 2.1, 2.8, and 1.08 respectively. These results will be related to the state of corrosion of the steel bars in section 3.5.

3.4 Visual inspection of corrosion specimens

The corrosion specimens were split open to release the embedded bars after 1750 days of exposure to the chloride induced corrosion environment which simulated realistic practical conditions for accelerated corrosion. Visual inspection of the corrosion was performed by 3D scanning the surface area of bars with an infinite focus optical system. Figure 14 shows the severity of corrosion on the surface of steel embedded in AACM 1,2,3 and PC concrete. No corrosion activity was observed on the surface of steel embedded in AACM 1 and 2 while the steel in AACM 3 had a slight stain of rust. The extent of corrosion on steel in PC concrete is significantly more pronounced (Fig.14). Corrosion protection to steel is provided by the oxidation of sulfide ions present in the pore fluid of the GGBS based AACM concrete. This forms a dark passive layer on the surface of the steel as observed in Figure 14.

Figure 14: Chloride induced corrosion of steel embedded in AACM and PC concrete after 1750 days exposure.

High values of E_{corr} and I_{corr} in AACM concrete are caused by sulfide concentration in the pore solution chemistry at the steel-concrete interface and not the actual corrosion resistance of the

embedded steel, as discussed in sections 3.2.1 and 3.2.2 respectively. In addition electrochemical test procedures such as open circuit potential, electrochemical impedance spectroscopy, linear polarization resistance and anodic polarization can also induce oxidation of HS^- species in AACM pore solution which result in high E_{corr} and I_{corr} readings [8]. Evidence of elemental sulfur (white flakes) from the oxidation of HS^- species in the pore solution is also observed in the matrix near the steel-concrete interface as shown in Figure 15 (discussed in section 3.2.2).

Figure 15: Elemental sulfur near the steel concrete interface in AACM 1 concrete after 1750 days exposure.

The passive film on the surface of steel embedded in GGBS-based AACM concrete is in the form of Fe-S complexes [8]. Structures of amorphous and crystalline oxides were also found on the steel surface embedded in AACM concrete such as an abundance of akageneite (β-FeO(OH,Cl)) and lepridocrocite (γ-FeO(OH), together with traces of maghemite (γ-Fe_2O_3) and goethite (αFeO(OH)) [53]. The presence of chloride found in akageneite (β-FeO(OH,Cl)) which is part of the passive oxide structure, forms a rarely observed protective film on the surface of steel embedded in AACM concrete [50].

3.5 Corrosion threshold values

Figure 15 shows a snapshot of the Cl^-/OH^- at 30mm depth (location of steel), I_{corr} and E_{corr} values for the AACM and PC concretes after 860 days of chloride induced corrosion exposure. Maximum chloride ingress would have occurred by this time since further exposure to chlorides is not provided after 690 days.

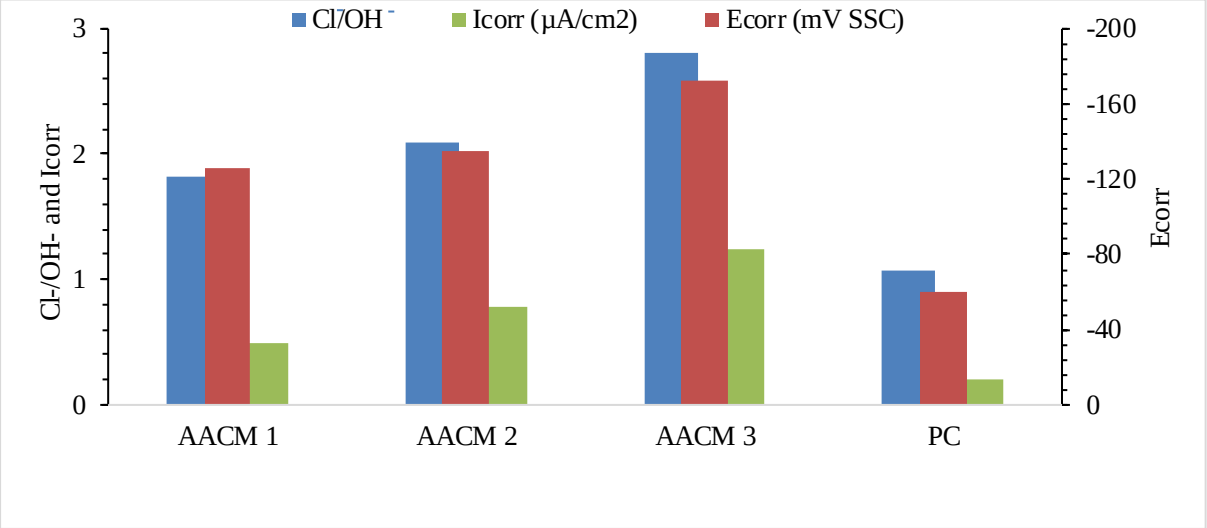

Figure 16: Relationship between potential, current density and Cl/OH at steel concrete interface (30mm depth) at 860 days exposure.

The Cl/OH values of the AACMs, which range between 1.82, 2.1 and 2.8, are much greater than 1.08 for PC concrete while the Icorr and Ecorr values for AACMs suggest much greater corrosion activity in the AACM concretes. AACM 3 has the highest E_{corr} and I_{corr} values of -172mV and 1.24µA/cm^2 while AACM 1, 2 and PC concrete have relatively lower values as shown in Fig. 16. Despite these observations, the extracted steel embedded in AACM 1 and 2 shows no signs of corrosion, AACM 3 concrete shows a few rust stains while steel in PC concrete shows quite extensive pitting corrosion (Figure 14). Other researchers [8, 12, 46] observed Cl^-/OH^- in AACM concrete exceeding the range of values which usually represent corrosion activity of steel embedded in PC concrete.

The historical Cl^-/OH^- threshold value of 0.61 [54] for the initiation of corrosion in PC based materials was based on simulated pore solution, neglecting the impact of chloride binding and buffering effect of the hydration product by releasing OH^- into the pore solution. Values of 3 and above have been given by tests using more representitive environments (45,54). Many recent researchers [5, 8, 14, 39] have similarly investigated corrosion of steel bars in simulated pore solutions of alkali-activated concrete while neglecting the influence of physical chloride binding [23, 35] and the redox environment [5] around the steel interface in AACM concrete. Various values of $Cl^-/OH^- \geq 1.0$ and $I_{corr} \geq 2.0$ have been given in literature for the onset of pitting corrosion in AACM concretes represented by idealised pore solutions of different molarity [5, 8]. Similarly, for ternary PC concrete containing GGBS, $Cl^-/OH^- \geq 1.64$, $I_{corr} \geq 6.1$ $\mu A/cm^2$ and $E_{corr} \leq -500mV$ shows the onset of pitting corrosion which is resisted by the presence of sulfide and thiosulfates from the slag content in the mix [32]. In this study, three different activator molarities of 6.5mol/L (AACM 1), 6.26mol/L (AACM 2) and 6.03mol/L (AACM 3) as shown in Table 1 played a significant role in the corrosion resistance of the AACM concrete. Onset of pitting corrosion was only observed in AACM 3 having an activator molarity of 6.03mol/L at Cl^-/OH^- of 2.8, I_{corr} of 1.24 $\mu A/cm^2$ and E_{corr} of -172 mV. AACM 1 concrete with activator molarity of 6.5mol/L did not show any pitting corrosion at Cl^-/OH^- of 1.82, I_{corr} of 0.5 $\mu A/cm^2$ and E_{corr} of -126 mV. Similarly, AACM 2 with activator molarity of 6.26mol/L did not show any pitting corrosion at Cl^-/OH^- of 2.1, I_{corr} of 0.78 $\mu A/cm^2$ and E_{corr} of -135 mV at 860 days exposure as shown in Figure 16.

CONCLUSIONS

The following conclusions can be drawn based on the study carried out on the chloride induced corrosion in AACM and a control PC concrete at 1750 days exposure to monitor their relative durability.

- Steel bars embedded in AACM concrete demonstrated a higher resistance to chloride induced corrosion than the corresponding control PC concrete after 1750 days of exposure to an accelerated corrosion inducing environment.
- Corrosion resistance of the AACM concretes increases with increasing molarity of the alkali activator, at a constant liquid to binder ratio. No pitting corrosion was detected at molarities 6.5 mol/L and 6.26 mol/L while a rust stain was observed at 6.03 mol/L. The control PC concrete displayed significant pitting corrosion.
- The threshold Cl^-/OH^- value for pitting corrosion initiation in the AACM concrete is between 2.1 and 2.8. No corrosion was detected in AACM concrete at Cl^-/OH^- ratios of 1.82 and 2.1 while a rust stain was observed at Cl^-/OH^- of 2.8 after 1750 days exposure. The corresponding threshold of corrosion initiation for the control PC concrete is around 1.08.
- AACM concrete also satisfies the nominal limit for acid soluble chloride content of 0.4% (by weight of binder) to prevent reinforcement corrosion, as stipulated in many standards for PC concrete. Steel reinforcement in the AACM concrete remained free from corrosion at chloride contents exceeding 0.4%. However, there is no basis for applying this threshold limit to AACM concrete.
- The alkalis Na^+, K^+, Al^{3+} and Mg^{2+} are more abundant in AACM than PC concrete. For example, their sum at 30mm depth in AACM 1,2,3 and PC concrete is 14.4%, 14.86%, 18.17% and 5.07% respectively. These alkalis contribute to the high alkalinity of AACM concrete, which also provides corrosion resistance to steel reinforcement. $Ca(OH)_2$ content, however, is lower in AACM (0%) than PC (5%) concrete.

- Corrosion protection to steel is provided by the oxidation of sulfide ions present in the pore fluid of GGBS based AACM concrete. The AACM concrete has up to 80% higher SO_3^{2-} content at the steel interface than PC concrete. The presence of sulfides reduces the redox reaction and deprives oxygen supply at the steel interface. This forms a dark passive layer on the surface of the steel which impedes corrosion.
- Corrosion potentials, E_{corr}, of steel in submerged AACM concrete reach very high negative values (-677 mV) without any signs of corrosion. This is due to the depletion of oxygen at the steel interface caused by the oxidation of sulfides present in AACM concrete and also the low oxygen levels available under submerged exposure. The corresponding E_{corr} values for the control PC remain fairly stable under submerged and dry exposure (0 to -250mV) and represent significant pitting corrosion.
- The E_{corr} and I_{corr} values of AACM concrete are highly influenced by the saturated state of the matrix. This is caused by the inhibition of the cathodic reaction in saturated AACM concrete producing higher I_{corr} and more negative E_{corr} values in non-corroding steel. It results in a lack of sufficient stability in these values under cyclic wet-dry exposure to provide a reliable corrosion indicator for the steel. However, the E_{corr} and I_{corr} values of AACM concrete remain fairly stable during prolonged partially saturated exposure.

ACKNOWLEDGMENTS

The authors gratefully acknowledge the support of the Materials and Engineering Research Institute, Sheffield Hallam University and the funding provided to the second author for postgraduate study by the Tertiary Education Trust Fund, Ministry of Education, Federal Republic of Nigeria. The authors also acknowledge the award by the UK - India Newton -

Bhabha programme through funding provided by Innovate UK, EPSRC (EP/P026206/1) and the Government of India for research on AACMs.

REFERENCES

1. O'Flaherty F, Mangat P, Lambert P, Brown EH (2010) Influence of shear reinforcement corrosion on the performance of under-reinforced concrete beams. Biophys. J.
2. Page C.L. and Lambert P. (1986) Analytical and Electrochemical Investigations of Reinforcement Corrosion. Crowthorne, Berkshire, UK
3. Gouda VK (1970) Corrosion and Corrosion Inhibition of Reinforcing Steel: I. Immersed in Alkaline Solutions. Br Corros J 5:198–203. https://doi.org/10.1179/000705970798324450
4. Ojedokun OO, Mangat PS (2016) Chloride diffusion in alkali activated concrete. In: II International Conference on Concrete Sustainability ICCS16, Madrid, Spain. pp 521–530
5. Mundra S, Criado M, Bernal SA, Provis JL (2017) Chloride-induced corrosion of steel rebars in simulated pore solutions of alkali-activated concretes. Cem Concr Res. https://doi.org/10.1016/j.cemconres.2017.08.006
6. Pourbaix M (1990) Thermodynamics and corrosion. Corros Sci. https://doi.org/10.1016/0010-938X(90)90205-J
7. Nishimura R. and Sato N. (1984) potential-pH diagram of composition/structure of passive film on iron. In: International congress on metallic corrosion. National council of canada, Toronto, pp 96–101
8. Mundra S, Bernal SA, Criado M, et al (2017) Steel corrosion in reinforced alkali-activated materials. RILEM Tech Lett. https://doi.org/10.21809/rilemtechlett.2017.39

9. Bertolini L, Elsener B, Pedeferri P, et al (2013) Corrosion of Steel in Concrete : Prevention, Diagnosis, Repair. Wiley
10. Ojedokun OO, Mangat PS (2018) Characterization and pore structure of rice husk ash cementitious materials. In: American Concrete Institute, ACI Special Publication
11. Lloyd RR, Provis JL, Van Deventer JSJ (2010) Pore solution composition and alkali diffusion in inorganic polymer cement. Cem Concr Res 40:2010. https://doi.org/10.1016/j.cemconres.2010.04.008
12. Ma Q, Nanukuttan S V., Basheer PAM, et al (2016) Chloride transport and the resulting corrosion of steel bars in alkali activated slag concretes. Mater Struct 49:3663–3677. https://doi.org/10.1617/s11527-015-0747-7
13. Criado M, Provis JL (2018) Alkali activated slag mortars provide high resistance to chloride-induced corrosion of steel. Front Mater. https://doi.org/10.3389/fmats.2018.00034
14. Tromans D (1980) Anodic Polarization Behavior of Mild Steel in Hot Alkaline Sulfide Solutions. J Electrochem Soc. https://doi.org/10.1149/1.2129865
15. El Haleem SMA, El Aal EEA (2008) Electrochemical behaviour of iron in alkaline sulphide solutions. In: Corrosion Engineering Science and Technology
16. Mangat PS, Ojedokun OO (2018) Influence of curing on pore properties and strength of alkali activated mortars. Constr Build Mater 188:. https://doi.org/10.1016/j.conbuildmat.2018.07.180
17. Angst U, Elsener B, Larsen CK, Vennesland O (2009) Critical chloride content in reinforced concrete - A review. Cem Concr Res 39:1122–1138. https://doi.org/10.1016/j.cemconres.2009.08.006
18. Galan I, Glasser FP (2015) Chloride in cement. Adv Cem Res 27:63–97.

https://doi.org/10.1680/adcr.13.00067

19. Shi X, Xie N, Fortune K, Gong J (2012) Durability of steel reinforced concrete in chloride environments: An overview. Constr. Build. Mater.
20. Kupwade-Patil K, Allouche EN, Vaidya S, Diaz-Loya EI (2012) Corrosion analysis of reinforced geopolymer concretes. Concr Solut
21. Gluth GJG, Arbi K, Bernal SA, et al (2020) RILEM TC 247-DTA round robin test: carbonation and chloride penetration testing of alkali-activated concretes. Mater Struct Constr. https://doi.org/10.1617/s11527-020-1449-3
22. BS EN 206 (2014) Concrete — Specification, performance, production and conformity. British Standards Institution
23. Mangat PS, Ojedokun OO (2019) Bound chloride ingress in alkali activated concrete. Constr Build Mater 212:375–387. https://doi.org/https://doi.org/10.1016/j.conbuildmat.2019.03.302
24. BS 882:1992 (1992) Specification for aggregates from natural sources for concrete. British Standards Institution
25. BS 4449:2005+A3:2016 Steel for the reinforcement of concrete. Weldable reinforcing steel. Bar, coil and decoiled product. Specification. British Standards Institution
26. The Concrete Society (2004) TR60 Electrochemical tests for reinforcement corrosion. Surrey
27. ASTM C876-09 (2009) Standard Test Method for Corrosion Potentials of Uncoated Reinforcing Steel in Concrete. ASTM B Stand. https://doi.org/10.1520/C0876-09.2
28. Nordtest 443 (1995) Hardened concrete: Accelerated chloride penetration. FIN-02150 ESPOO, Finland
29. BS EN 12390-11:2015 Testing hardened concrete. Determination of the chloride

resistance of concrete, unidirectional diffusion. British Standards Institution

30. Barneyback RS, Diamond S (1981) Expression and analysis of pore fluids from hardened cement pastes and mortars. Cem Concr Res. https://doi.org/10.1016/0008-8846(81)90069-7

31. Vollpracht A, Lothenbach B, Snellings R, Haufe J (2016) The pore solution of blended cements: a review. Mater Struct Constr. https://doi.org/10.1617/s11527-015-0724-1

32. Scott A, Alexander MG (2016) Effect of supplementary cementitious materials (binder type) on the pore solution chemistry and the corrosion of steel in alkaline environments. Cem Concr Res. https://doi.org/10.1016/j.cemconres.2016.08.007

33. Macphee DE, Cao HT (1993) Theoretical description of impact of blast furnace slag (BFS) on steel passivation in concrete. Mag Concr Res. https://doi.org/10.1680/macr.1993.45.162.63

34. Csákberényi-Malasics D, Rodriguez-Blanco JD, Kis VK, et al (2012) Structural properties and transformations of precipitated FeS. Chem Geol. https://doi.org/10.1016/j.chemgeo.2011.12.009

35. Mangat PS, Ojedokun OO (2020) Free and bound chloride relationships affecting reinforcement cover in alkali activated concrete. Cem Concr Compos 103692. https://doi.org/10.1016/j.cemconcomp.2020.103692

36. Ke X, Bernal SA, Provis JL (2017) Uptake of chloride and carbonate by Mg-Al and Ca-Al layered double hydroxides in simulated pore solutions of alkali-activated slag cement. Cem Concr Res. https://doi.org/10.1016/j.cemconres.2017.05.015

37. Mees F, Tursina T V. (2018) Salt Minerals in Saline Soils and Salt Crusts. In: Interpretation of Micromorphological Features of Soils and Regoliths

38. Ojedokun OO and, Mangat PS (2019) Suitability of phenolphthalein indicator method

for alkali activated concrete. In: ICSBM 2019 2nd International Conference of Sustainable Building Materials. pp 363–372

39. Ahlström J, Tidblad J, Tang L, et al (2018) Electrochemical properties of oxide scale on steel exposed in saturated calcium hydroxide solutions with or without chlorides. Int J Corros. https://doi.org/10.1155/2018/5623504

40. Li PP, Brouwers HJH, Chen W, Yu Q (2020) Optimization and characterization of high-volume limestone powder in sustainable ultra-high performance concrete. Constr Build Mater. https://doi.org/10.1016/j.conbuildmat.2020.118112

41. Wu Z, Shi C, Khayat KH (2016) Influence of silica fume content on microstructure development and bond to steel fiber in ultra-high strength cement-based materials (UHSC). Cem Concr Compos. https://doi.org/10.1016/j.cemconcomp.2016.05.005

42. Zhang ST, Dou Y, Zhou J, et al (2016) DFT-Based Simulation and Experimental Validation of the Topotactic Transformation of MgAl Layered Double Hydroxides. ChemPhysChem. https://doi.org/10.1002/cphc.201600354

43. Holloway M, Sykes JM (2005) Studies of the corrosion of mild steel in alkali-activated slag cement mortars with sodium chloride admixtures by a galvanostatic pulse method. Corros Sci 47:3097–3110. https://doi.org/10.1016/j.corsci.2005.05.035

44. Bastidas DM, Fernández-Jiménez A, Palomo A, González JA (2008) A study on the passive state stability of steel embedded in activated fly ash mortars. Corros Sci 50:1058–1065. https://doi.org/10.1016/j.corsci.2007.11.016

45. Poursaee A, Hansson CM (2009) Potential pitfalls in assessing chloride-induced corrosion of steel in concrete. Cem Concr Res 39:391–400. https://doi.org/10.1016/j.cemconres.2009.01.015

46. Babaee M, Castel A (2016) Chloride-induced corrosion of reinforcement in low-

calcium fly ash-based geopolymer concrete. Cem Concr Res 88:96–107. https://doi.org/10.1016/j.cemconres.2016.05.012

47. Monticelli C, Natali ME, Balbo A, et al (2016) Corrosion behavior of steel in alkali-activated fly ash mortars in the light of their microstructural, mechanical and chemical characterization. Cem Concr Res. https://doi.org/10.1016/j.cemconres.2015.11.001
48. Lambert P, Page CL, Vassie PRW (1991) Investigations of reinforcement corrosion. 2. Electrochemical monitoring of steel in chloride-contaminated concrete. Mater Struct 24:351–358. https://doi.org/10.1007/BF02472068
49. Neugebauer H, Tschinkel W, Nauer G, Neckel A (1988) In-situ FTIR spectroscopy of iron electrodes. Mikrochim Acta. https://doi.org/10.1007/BF01205886
50. Monticelli C, Natali ME, Balbo A, et al (2016) A study on the corrosion of reinforcing bars in alkali-activated fly ash mortars under wet and dry exposures to chloride solutions. Cem Concr Res. https://doi.org/10.1016/j.cemconres.2016.05.010
51. Sumranwanich T, Tangtermsirikul S (2004) A model for predicting time-dependent chloride binding capacity of cement-fly ash cementitious system. Mater Struct 37:387–396. https://doi.org/10.1007/BF02479635
52. Neville AM (2011) Properties of Concrete. Pearson Education Limited
53. Moreno JD, Bonilla M, Adam JM, et al (2015) Determining corrosion levels in the reinforcement rebars of buildings in coastal areas. A case study in the Mediterranean coastline. Constr Build Mater. https://doi.org/10.1016/j.conbuildmat.2015.09.059
54. Hausmann DA (1967) Steel corrosion in concrete -- how does it work? Mater Prot 6:19–23